

A novel antitumor peptide inhibits proliferation and migration and promotes apoptosis in glioma cells by regulating the MKK6/p38 signaling pathway

Rong WANG^{1,2,*}, Bo-Wen LI^{2,*}, Nai-Yuan SHAO¹, Dan-Ni DENG², Feng ZHI^{1,2,*}

¹Department of Neurosurgery, The First People's Hospital of Changzhou, Changzhou, Jiangsu, China; ²Clinical Medical Research Center, The Third Affiliated Hospital of Soochow University, Changzhou, Jiangsu, China

*Correspondence: danielzhif@suda.edu.cn

*Contributed equally to this work.

Received November 9, 2020 / Accepted February 19, 2021

Protein- or peptide-based therapeutics have emerged as an innovative strategy for the treatment of cancer. Our previous research demonstrated that tripartite motif 9 short isoform (TRIM9s) is a tumor suppressor in glioma. In this report, we investigated whether a new peptide derived from TRIM9s, named T9sP, inhibits glioma progression and determined the possible molecular mechanism. The CCK-8 proliferation assay was performed in LN229 and U251 glioma cells. The scratch-wound assay was used to determine the migration of the cells. Apoptosis was assessed by flow cytometry using Annexin V-FITC/PI double staining method. The relative protein expression levels were detected by immunoblot analysis. The cell-penetrating peptide TAT was fused with T9sP to form TAT-T9sP. TAT-T9sP efficiently penetrated through the cell membrane of both LN229 and U251 cells. TAT-T9sP inhibited proliferation and migration and promoted apoptosis of glioma cells. TAT-T9sP activated p38 signaling by upregulating MKK6, and a p38 inhibitor, SB203580, reversed the inhibitory effects of TAT-T9sP on glioma cells. These results indicated the potential of TAT-T9sP for the development of a new anti-glioma medicine.

Key words: T9sP, glioma, p38, MKK6

Glioma is a primary malignant intracranial tumor that accounts for 50–60% of primary tumors of the central nervous system (CNS) [1]. According to the glioma classification criteria of the World Health Organization (WHO), glioblastoma (GBM) is the most malignant type of glioma and accounts for approximately 56% of glioma [2]. The annual incidence of GBM is approximately 6/100,000 worldwide, and it has increased over the last ten years [3, 4]. GBM patients usually have a poor prognosis with a median survival of approximately 10 months [5]. Despite recent advances in multiple combined therapies, including maximal surgical resection and chemoradiotherapy, the survival rate of GBM patients remains low [6–8]. Thus, the investigation of novel effective therapeutic strategies for the treatment of glioma is needed and is challenging.

Recently, protein/peptide therapeutics have emerged as a new strategy for treating multiple cancers [9]. Proteins/peptides are a group of important therapeutic agents with unique advantages, such as high specificity, low toxicity, and easy manipulation [10]. The p53p-Ant peptide, composing the COOH-terminal peptide of p53 and truncated homeobox

domain of Antennapedia (Ant), inhibited cell proliferation by inducing rapid apoptosis in a Fas-dependent manner in glioma cell lines [11]. The synthetic peptide LyeTxI-b inhibited cell growth, increased autophagy, disrupted cell membrane integrity, and induced necrosis in glioma cell lines and showed mild cytotoxicity in several non-tumor cell lines [12]. The anticancer activity of the Dermaseptin-PS1 peptide involved the disruption of the cell membrane and induction of intrinsic apoptosis in glioma [13]. A combination of vicrystatin plus temozolomide was effective in the treatment of intracranial glioma in mice [14]. Several peptides have been used to treat glioma; however, novel peptides, which may potentially be developed into new drugs, are still needed.

In our previous study on the molecular function of TRIM9 in glioma, we made an interesting observation [15]. TRIM9 has two isoforms, the full-length TRIM9, named TRIM9L (700 amino acids), and the short isoform of TRIM9, named TRIM9s (550 amino acids). TRIM9s, and not TRIM9L, suppressed glioma progression by mutual stabilization with MKK6 to potentiate the p38 signaling. Furthermore, TRIM9s could interact with MKK6, while

TRIM9I, TRIM9I-SD (TRIM9I minus the shared domain with TRIM9s), or TRIM9I-UD (TRIM9I minus the unique domain of TRIM9I) did not interact with MKK6 [15]. This observation suggested that the antitumor effect of TRIM9s on glioma may be due to a specific sequence of TRIM9s (TSEGKALQYPSERELRGI), named T9sP. As protein/peptide cargoes usually have relatively low cell membrane permeability, the cell-penetrating peptide (CPP) TAT (GGRKKRRQRRR), a commonly used short peptide for drug delivery in glioma [16], was utilized to facilitate the intracellular delivery of T9sP. In the present paper, our main objective is to survey the biological effects and the underlying molecular mechanisms of TAT-T9sP in glioma.

Materials and methods

Chemicals and reagents. T9sP, FITC-T9sP, TAT-T9sP, FITC-TAT-T9sP, scrambled control peptide (Scr, GQLYEAQRKKGITEPSSRL) generated by the permutation of T9sP sequence, FITC-Scr, TAT-Scr, and FITC-TAT-Scr were designed and synthesized by Beierbo (Nanjing, China). Ultra-high performance liquid chromatography (HPLC) system was performed to purify all the peptides, resulting in purity >98%. Dulbecco's modified eagle medium (DMEM), phosphate-buffered saline (PBS, pH 7.4), fetal bovine serum (FBS), penicillin-streptomycin-glutamine (100×), and trypsin contains EDTA and phenol red (0.25%) were purchased from Thermo Fisher Scientific (Waltham, MA, USA). Peptide stocks (10 mM) were prepared in PBS and stored in aliquots at -80 °C until use. A p38 inhibitor (SB203580) was obtained from Selleck (Houston, Texas, USA). The primary antibodies, including phosphorylated p38 MAP kinase (#9211), p38 MAP kinase (#8690), phosphorylated ERK1/2 (#9101), ERK1/2 (#9102), phosphorylated JNK (#9251), JNK (#9252), and β -actin (#4970) were obtained from Cell Signaling Technology (Danvers, MA, USA). MKK6 antibody (51094-1-AP) was purchased from Proteintech (Hubei, China). The secondary antibody (peroxidase affinity-purified goat anti-rabbit IgG, 111-035-003) was obtained from Jackson Immuno-Research (PA, USA).

Cell culture. The normal human glial cell line HEB was obtained from Beierbo (Nanjing, China). The human GBM cell lines including LN229 and U251 were purchased from the Cell Bank of the Chinese Academy of Sciences (Shanghai, China). Complete medium (DMEM supplemented with 10% FBS and 1% antibiotics) was used for supporting the growth of all the cell lines. Cells were cultured under the same conditions, including humidified air, 5% CO₂ concentration, and 37 °C constant temperature. Cells, in the log phase of growth, were chosen for the following experiments.

In vitro cellular uptake. LN229 and U251 cells were seeded in 6-well cell culture plates upon reaching 70% confluence. All the cell lines were treated with FITC-Scr, FITC-TAT-Scr, FITC-T9sP, or FITC-TAT-T9sP, respectively. After 24 h of incubation, the cells were evaluated under a fluorescence

microscope (Olympus IX71, Tokyo, Japan). Furthermore, the amount of intracellular green fluorescence was determined by using a Guava EasyCyte 6HT-2L flow cytometer (Millipore, Boston, USA).

Cell proliferation assay. To detect cell proliferation, a cell counting kit-8 (CCK-8) assay (Beyotime, Shanghai, China) was performed as described by experimental instructions of the manufacturer. All the cell lines (HEB, LN229, and U251 cells) were seeded in 96-well cell culture plates at optimum density in 100 μ l of culture medium, and then treated with a series of different concentrations of TAT-Scr, TAT-T9sP, or TAT-T9sP plus SB203580 for 24 h. 10 μ l of CCK-8 solution was added to each well and the plates were incubated in the 37 °C incubator for 1 h. The absorbance was determined at 450 nm by a Synergy 2 microplate reader (BioTek, Winooski, USA).

Wound healing assay. The LN229 and U251 (1 \times 10⁵ cells/well) glioma cells were seeded in 6-well cell culture plates and were allowed to completely adhere overnight. A consistent wound gap between the cells was generated by a disposable pipette tip. Subsequently, the cells were washed with PBS and exposed to TAT-Scr, TAT-T9sP, or TAT-T9sP plus SB203580 for 24 h. The wound was photographed using a phase-contrast microscope (Olympus IX71, Tokyo, Japan), and the wound field was quantified and expressed using the ImageJ software. The relative migration rate was evaluated according to the equation: The percent wound closure (%) = [wound distance (0 h) - wound distance (n h)]/wound distance (0 h) \times 100%.

Migration assay. The cell migration assay was performed using Transwell plates (BD, New Jersey, USA) as previously reported [17]. The pictures were photographed in six randomly selected fields under the microscope with Image-Pro Insight software (Olympus IX71, Tokyo, Japan).

Cell apoptosis assay. The cells were collected after TAT-Scr, TAT-T9sP, or TAT-T9sP plus SB203580 treatment for 24 h. Then, the Annexin V-FITC/propidium iodide (PI) flow cytometric analysis was performed to identify the apoptotic cells. The collected cells were washed with cold PBS and centrifuged at 1000 \times g for 5 min. The supernatant was discarded, the cells were resuspended in Annexin V-FITC binding solution and then stained with Annexin V-FITC and PI (Beyotime, Shanghai, China) in the dark for 20 min at room temperature (20-25 °C). The apoptotic cells were investigated by flow cytometry on a Guava EasyCyte 6HT-2L instrument.

Western blot. The cells treated with peptides were lysed with ice-cold RIPA lysis buffer (MultiSciences Biotech, China) at the indicated time points. The protein content was assayed by using the bicinchoninic acid (BCA) method. The proteins were denatured by loading buffer at 100 °C for 5 min, and equal amounts of protein were loaded onto sodium dodecyl sulfate-polyacrylamide gel electrophoresis (SDS-PAGE) gel. Immediately afterward, the proteins were electrotransferred to polyvinylidene difluoride (PVDF) membranes at 350 mA. The membranes were incubated with blocking buffer for 1 h

at room temperature followed by incubated with antibodies against MAPKs, MKK6, or β -actin at the optimal dilution with gentle agitation overnight at 4°C. After washed three times, the membranes were incubated with the secondary antibody for 1 h at room temperature. Finally, the immunoreactive proteins were observed using standard ECL substrates (Thermo, USA) by a Tanon-4600 imaging system (Tanon, Shanghai, China).

Statistical analysis. All experiments were repeated at least three times and the data are shown as the mean \pm standard deviation (SD). Statistical analysis of group comparison was determined by GraphPad Prism 5.0 software. The differences between two groups and multi-groups were analyzed with unpaired Student's t-test and one-way ANOVA followed by Tukey analysis, respectively. The significance of differences was at p-value of <0.05.

Results

TAT-T9sP peptide and *in vitro* uptake. To enhance the transmembrane permeability, the T9sP peptide or Scr peptide was fused with TAT to form TAT-T9sP or TAT-Scr, respectively, as illustrated in Figure 1A. The peptide had a purity > 98% and a molecular mass of 3598.1 Da according to the UHPLC analysis (Supplementary Figure S1A) and mass spectrometry, respectively (Supplementary Figure S1B). To monitor the uptake, fluorescein isothiocyanate (FITC) was used to label TAT-T9sP or TAT-Scr to generate FITC-TAT-T9sP or FITC-TAT-Scr. The cells were incubated with FITC-Scr, FITC-TAT-Scr, FITC-T9sP, or FITC-TAT-T9sP for 24 h, and fluorescence microscopy was used to analyze the cellular internalization of these peptides. As shown in Figure 1B, strong green fluorescence was observed in the cells exposed to FITC-TAT-Scr and FITC-TAT-T9sP, and low green fluorescence was detected in the cells exposed to FITC-Scr and FITC-T9sP. This observation was also confirmed by a flow cytometry experiment. As shown in Figures 1C–1F, the green fluorescence intensity was significantly enhanced in the cells treated with FITC-TAT-Scr and FITC-TAT-T9sP and was barely increased in the cells treated with FITC-Scr and FITC-T9sP. As Scr and T9sP were unable to efficiently penetrate the cell membrane, TAT-Scr and TAT-T9sP were used in the subsequent experiments. These results suggested that TAT-T9sP could penetrate through the cell membrane.

TAT-T9sP inhibited cell proliferation and migration and promoted cell apoptosis. To determine the antitumor effects of TAT-T9sP on glioma, different concentrations of TAT-T9sP were added to HEB, LN229, and U251 cells. The CCK-8 assay results indicated that TAT-T9sP was not cytotoxic to HEB cells (Figure 2A). The viability of LN229 cells treated with TAT-T9sP was gradually decreased in a dose-dependent manner, and TAT-Scr was not cytotoxic to the LN229 cells (Figure 2B). The IC₅₀ value of TAT-T9sP in LN229 cells was 350.2 μ M (Supplementary Figure S2A).

The viability of U251 cells treated with TAT-T9sP was also diminished in a clear dose-dependency, and TAT-Scr was not cytotoxic to U251 cells (Figure 2C). The IC₅₀ value of TAT-T9sP in U251 cells was 206.7 μ M (Supplementary Figure S2B). As TAT-T9sP was cytotoxic in LN229 cells at a concentration of 40 μ M and in U251 cells at a concentration of 20 μ M, the TAT-T9sP concentration of 40 μ M was chosen for the following experiments.

Cell migration is an essential stage for cancer metastasis; hence, the effect of TAT-T9sP on cell migration was examined using the scratch-wound assay. The wound closure was almost complete at 48 h in LN229 cells treated with TAT-Scr, and the wound was partially closed at 48 h in LN229 cells treated with TAT-T9sP as shown in Figure 2D. The relative migration rate was statistically analyzed as shown in Figure 2E. Similar to the observations in LN229 cells, TAT-T9sP, but not TAT-Scr, significantly inhibited the migration of U251 cells as shown in Figure 2F. The statistical analysis of the relative migration rate in U251 cells was shown in Figure 2G. The Transwell migration assay was also performed to evaluate the effect of TAT-T9sP on cell migration. As shown in Figure 2H, compared with TAT-Scr, TAT-T9sP significantly inhibited the migration of LN229 and U251 cells. The statistical analysis results of the relative migration rate in LN229 and U251 cells are shown in Figures 2I and 2J.

Furthermore, the effect of TAT-T9sP on apoptosis was examined using the FITC-Annexin V/PI assay. As shown in Figures 2K and 2L, TAT-T9sP treatment increased the average ratio of cells that were in early apoptosis from 3.84% to 20.44%, and the average ratio of cells that were in late apoptosis or already dead was increased from 2.08% to 4.44% in LN229 cells. As shown in Figures 2M and 2N, TAT-T9sP treatment increased the average ratio of cells that were in early apoptosis from 3.31% to 22.04%, and the average ratio of cells that were in late apoptosis or already dead was increased from 3.85% to 8.99% in U251 cells. However, no significant changes were observed in LN229 and U251 cells treated with TAT-Scr.

TAT-T9sP activated p38 signaling by upregulating MKK6. According to our previous reports, TRIM9s suppresses GBM progression by stabilizing MKK6 to enhance p38 signaling; thus, we sought to determine whether the TAT-T9sP peptide derived from TRIM9s influences the MKK6/p38 axis. The levels of MKK6 and p-p38 were significantly increased after TAT-T9sP treatment, and SB203580 significantly reversed this effect in LN229 cells (Figure 3A). The statistical analysis is shown in Figures 3B and 3C. Similar results were detected in U251 cells, as shown in Figure 3D. The statistical analysis is shown in Figures 3E and 3F. Then, we investigated whether TAT-T9sP influences other MAPKs. As shown in Figures 3G–3I, small changes in the protein levels of ERK, p-ERK, JNK, and p-JNK were detected after the cells were treated with TAT-T9sP. These results suggested that TAT-T9sP activated p38 signaling by upregulating MKK6.

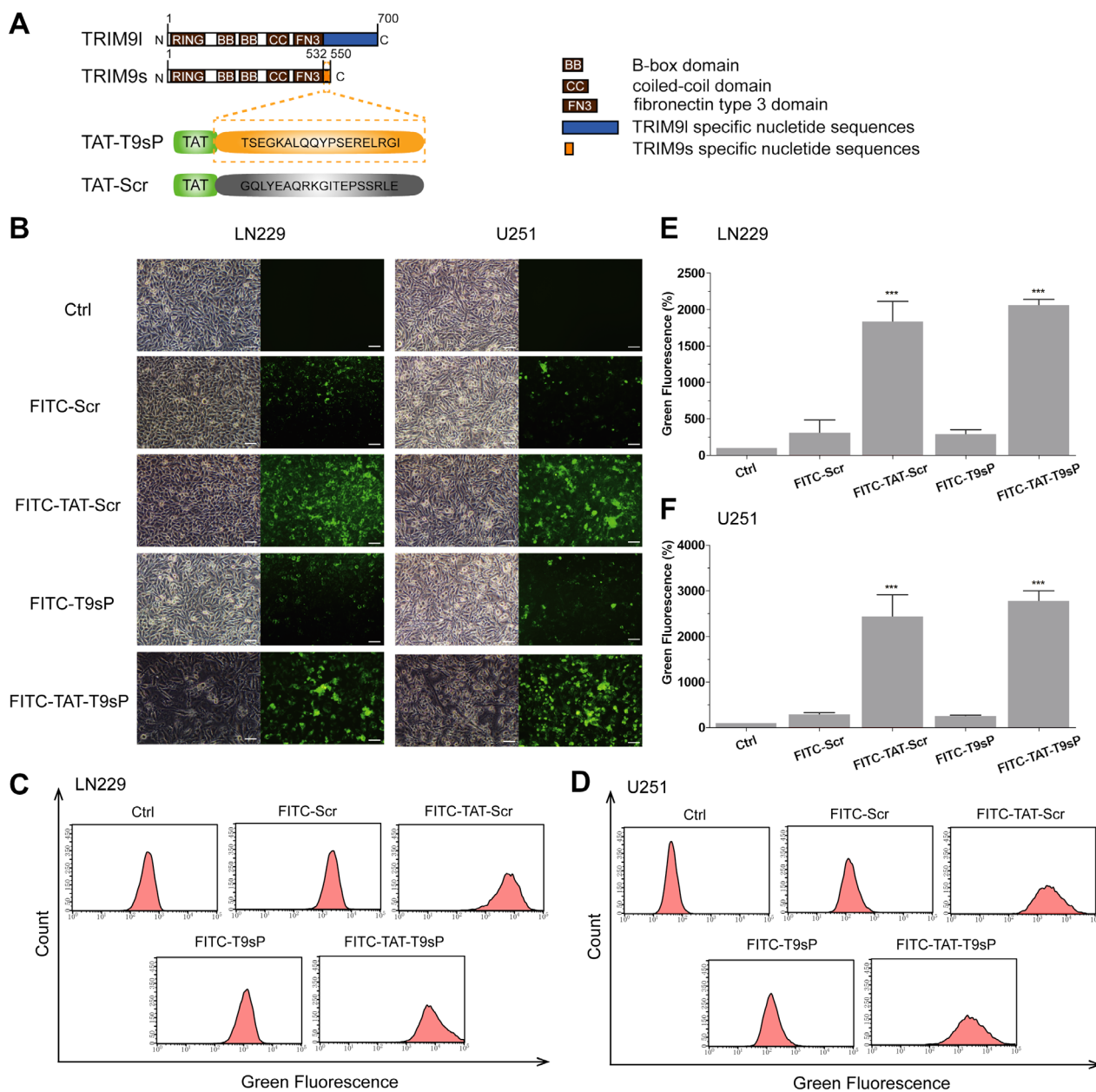


Figure 1. Peptide design and cellular uptake *in vitro*. **A**) Scheme of the structure of TAT-T9sP and TAT-Scr. **B**) The cells were treated with PBS as the control group (Ctrl), FITC-Scr, FITC-TAT-Scr, FITC-T9sP, or FITC-TAT-T9sP for 24 h, and representative cell images were captured under a fluorescence microscope (with phase-contrast as a control). Scale bars, 100 μ m. **C, D**) The green fluorescence intensity in the cells after different treatments assayed by flow cytometry. **E, F**) Statistical analysis of the fluorescence intensity in cells determined by flow cytometry. *** $p < 0.001$ vs. Ctrl

SB203580 reversed the inhibitory effects of TAT-T9sP on glioma. TAT-T9sP inhibited tumor progression and activated p38 signaling in glioma; thus, we examined if the inhibitory effect of TAT-T9sP is dependent on p38 activation. SB203580, a specific ATP-competitive inhibitor of p38 MAPK, was used to inhibit p38 activation. SB203580 abolished the inhibitory effect of TAT-T9sP on cell proliferation in LN229 cells as shown in Figure 4A and in U251

cells as shown in Figure 4B. The IC_{50} value of TAT-T9sP was upregulated from 350.2 μ M to 412.9 μ M in LN229 cells after SB203580 treatment (Supplementary Figure S2C). The IC_{50} value of TAT-T9sP was upregulated from 206.7 μ M to 270.4 μ M in U251 cells after SB203580 treatment (Supplementary Figure S2D). Moreover, SB203580 attenuated the inhibitory effect of TAT-T9sP on cell migration in LN229 cells as shown in Figure 4C–D and in U251 cells as shown in Figures 4E

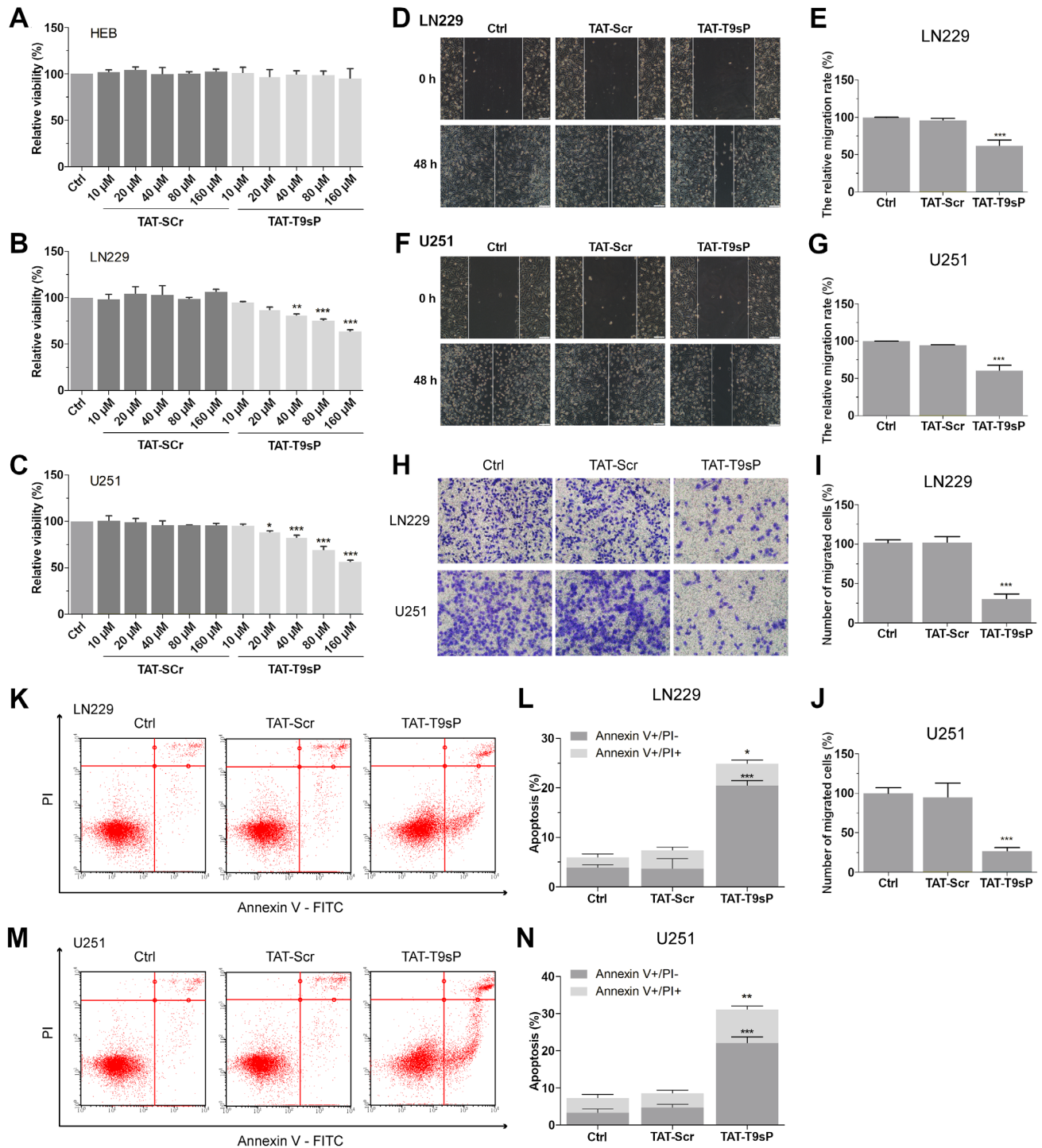


Figure 2. TAT-T9sP inhibited cell proliferation and migration and promoted cell apoptosis. A–C) The relative cell proliferation was determined by a CCK-8 assay in HEB, LN229, and U251 cells after different treatments. D) The representative images of migration in LN229 cells by the scratch-wound assay. Scale bar, 200 μ m. E) The relative migration rate in LN229 cells was quantified. F) The representative images of migration in U251 cells by the scratch-wound assay. Scale bar, 200 μ m. G) The relative migration rate in U251 cells was quantified. H) The Transwell migration assay was performed in LN229 and U251 cells. I) Relative migrated cells in LN229 cells were statistically analyzed. J) Relative percent of migrated cells in U251 cells was statistically analyzed. K) The apoptosis of LN229 cells treated with TAT-T9sP or TAT-Scr was assessed using flow cytometry and representative images are shown. L) Statistical analysis of the percent of apoptotic cells in LN229 cells. M) Apoptosis of U251 cells treated with TAT-T9sP or TAT-Scr was assessed using flow cytometry and representative images are shown. N) Statistical analysis of the percent of apoptotic cells in U251 cells. * $p < 0.05$, ** $p < 0.01$, *** $p < 0.001$ vs. Ctrl

and 4F. SB203580 also released the inhibitory effect of TAT-T9sP on cell migration as indicated in the Transwell migration assay in LN229 cells and in U251 cells as shown in Figures 4G–4I. Furthermore, SB203580 decreased enhanced apoptosis induced by TAT-T9sP in LN229 cells as shown in Figures 4J–4K and in U251 cells as shown in Figures 4L and 4M. These results confirmed that the inhibition of TAT-T9sP on glioma was dependent strongly on p38 activation.

Discussion

Chemotherapy with temozolomide (TMZ), bis-chloroethyl nitrosourea (BCNU), or other cytotoxic agents is a critical part of the standard treatment for GBM [18]. Despite the advances in GBM knowledge and therapeutic drug development, the prognosis of GBM patients remains poor [5]. In this research, the antitumor effect of a novel peptide TAT-T9sP was examined in glioma *in vitro*. TAT-T9sP inhibited cell proliferation and migration and promoted cell apoptosis by upregulating MKK6 to potentiate the p38 signaling pathway in glioma. These results indicated the potential of TAT-T9sP to be developed into a new anti-glioma medicine.

During the last decade, the use of protein/peptide drugs was the crucial strategy for treating cancer [19]. Compared with chemotherapy and gene therapy, protein/peptide drugs have many advantages such as high specificity, high tolerance, low toxicity, and low genotoxicity [20]. Furthermore, advances in protein engineering and molecular modeling enabled the easy manipulation and application of peptides with short amino acid sequences, thus making them more suitable for clinical use [21]. The peptide FNIII14 is able to suppress cell survival, potentiate TMZ cytotoxicity, and downregulate O⁶-methylguanine-DNA methyltransferase (MGMT) levels via the inactivation of integrins *in vitro* and *in vivo* in glioma [22]. Epinecidin-1, an antimicrobial peptide (AMP), promotes mitochondrial hyperpolarization, causes DNA damage, and increases reactive oxygen species (ROS) generation to induce cell death in GBM [23]. The AMP tilapia piscidin 4 (TP4) induces cell cytotoxicity by impairing mitochondria and elevating intracellular ROS in GBM [24]. In the present study, the T9sP derived from the C-terminus of TRIM9s was confirmed as an effective antitumor peptide. T9sP inhibits cell proliferation and migration and promotes cell apoptosis by upregulating MKK6 to potentiate the p38 signaling.

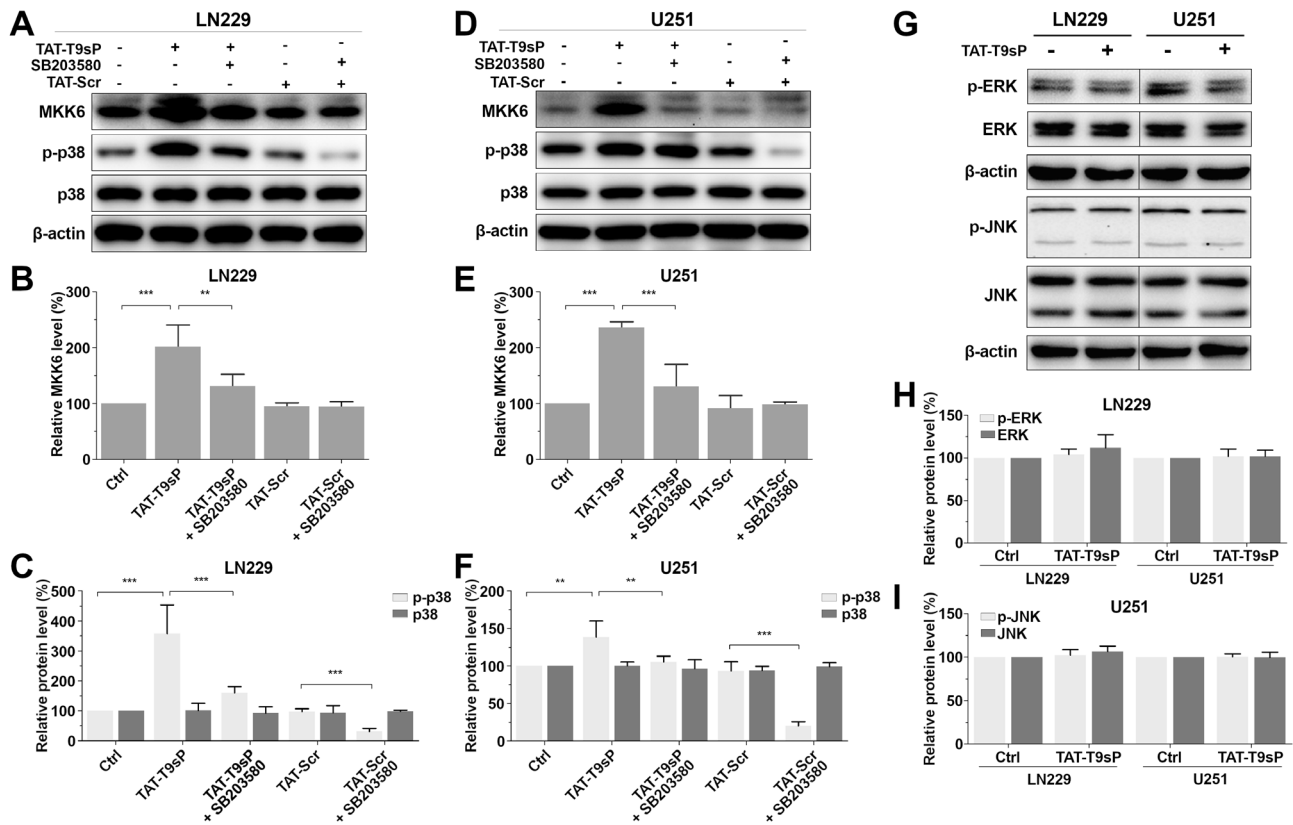


Figure 3. TAT-T9sP activated p38 signaling by upregulating MKK6. A) The protein expression levels of MKK6, p-p38, and p38 in LN229 cells after indicated treatments. B) Quantification of MKK6 protein changes. C) Quantification of p-p38 and p38 protein changes. D) The protein expression levels of MKK6, p-p38, and p38 in U251 cells after treatments. E) Quantification of MKK6 protein changes. F) Quantification of p-p38 and p38 protein changes. G) Representative images of the proteins (p-ERK, ERK, p-JNK, and JNK) in LN229 and U251 cells after different treatments. H) Quantification of p-ERK and ERK protein changes. I) Quantification of p-JNK and JNK protein changes. * $p < 0.05$, ** $p < 0.01$, *** $p < 0.001$ vs. Ctrl

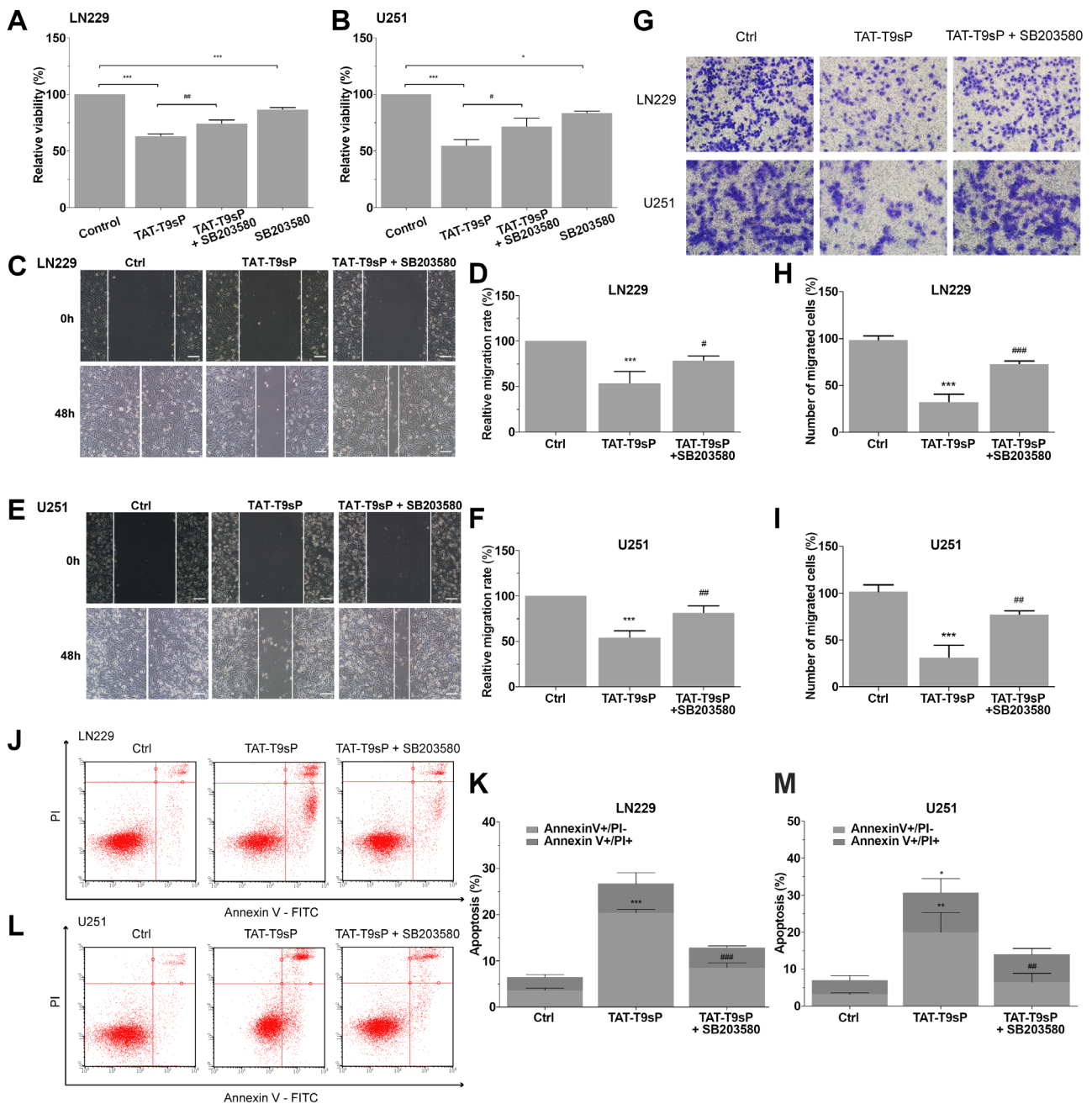


Figure 4. SB203580 reversed the inhibitory effects of TAT-T9sP on glioma. **A, B)** The cell proliferation was determined by the CCK-8 assay in the cells after different treatments. **C)** The migration was evaluated by the scratch-wound assay in LN229 cells. Scale bar, 200 μ m. **D)** Quantification of the relative migration rate in LN229 cells. **E)** The cell migration was examined by the scratch wound healing assay in U251 cells, scale bar, 200 μ m. **F)** Quantification of the relative migration rate in U251 cells. **G)** The cell migration was examined by the Transwell migration assay in LN229 and U251 cells. **H)** Relative percent of migrated cells in LN229 cells was statistically analyzed. **I)** Relative percent of migrated cells in U251 cells was statistically analyzed. **J, K)** The apoptosis of LN229 cells was assessed by flow cytometry and quantification was performed. **L, M)** The cellular apoptosis of U251 cells was determined by flow cytometry and quantification was performed. * $p < 0.05$, ** $p < 0.01$, *** $p < 0.001$ vs. Ctrl. # $p < 0.05$, ## $p < 0.01$, ### $p < 0.001$ vs. the TAT-T9sP-treated group

One of the main obstacles to the efficacy of active proteins/peptides in tumor cells is low cell permeability [25]. Various drug delivery systems, such as lipid-based membrane nanocarriers, polymeric carriers, and inorganic

vehicles, have been designed to enhance the cell permeability of these active proteins/peptides. An angiopep-2-functionalized lipid-based nanovector encapsulating nutlin-3a and iron oxide nanoparticles could penetrate the blood-brain barrier

(BBB) and selectively promote GBM cell death [26]. A polycationic liposomal polyethyleneimine and polyethylene glycol complex (LPPC) was developed to protect and deliver n-butyridene phthalide (BP) into brain tumor sites. The BP/LPPC was able to cross the BBB and decrease tumor volume by ameliorating cell cycle arrest and triggering cell apoptosis [27]. The PL3 peptide, which interacts with tenascin C, was proven to enhance the function of an iron oxide nanoworm and suppress GBM [28]. A ¹⁸F-VAP-modified liposome containing MTI-31 is efficiently internalized by tumor cells and suppresses GBM proliferation *in vitro* and *in vivo* [29]. Chlorotoxin (CTX) is a highly specific peptide targeting chloride channels (ClC-3) and matrix metalloproteinase (MMP-2), which are overexpressed in glioma tumor cells. CTX-conjugated PLGA nanoparticles containing morusin are able to inhibit cell proliferation and promote apoptosis *in vitro* [30]. A novel drug delivery system composed of red blood cell (RBC) membrane, drug nanocrystals (NCs), and a tumor-targeting RGD peptide selectively delivers NCs to glioma with high specificity and enhanced antitumor efficacy [31]. A cell-penetrating peptide R8-conjugated liposomes (R8PLP), efficiently cross BBB and deliver doxorubicin to the tumor region, leading to reduced tumor growth *in vivo* and *in vitro* [32]. In the present study, CPP TAT was fused to T9sP to form TAT-T9sP. TAT-T9sP efficiently penetrated the cell membrane to enter the cytoplasm and inhibit cell growth.

Although our results indicated the possible future use of TAT-T9sP as a novel antitumor peptide in glioma, our research has some limitations. 1) The cytotoxicity of T9sP in glioma was relatively low. The IC₅₀ value of T9sP in LN229 cells was 350.2 μM, and the IC₅₀ value in U251 cells was 206.7 μM. Compared with other antitumor peptides used in glioma [11–13], it seems that the antitumor effect of T9sP was mild. This phenomenon may be explained by a lack of optimization of T9sP. Peptide optimization is a critical step in the design and development of novel peptide drugs [33]. The sequence of T9sP was originally derived from the protein sequences different between TRIM9s and TRIM9l according to different biological functions of the proteins described in our previous report [15]. Thus, T9sP may need additional optimization, such as amino acid replacement, peptide length adjustment, and special chemical modifications [34]. 2) The T9sP delivery strategy was not fully investigated. In the present study, only the CPP TAT was fused with the T9sP peptide. The T9sP peptide may be delivered through various protein delivery systems, such as liposomes, DNA nanostructures, micelles, or nanogels [35]. 3) The molecular mechanism of the effect of T9sP against glioma was not fully investigated. The results demonstrated that T9sP inhibited glioma progression through MKK6 stabilization and p38 potentiation; however, the results are preliminary. For example, what is the mechanism by which T9sP stabilizes MKK6? Can T9sP influence other signaling pathways? What is the precise role of p38 in the effects of T9sP against glioma? 4) The antitumor effect of T9sP was not investigated *in vivo*.

The present study was performed only in cell lines *in vitro*. It is unknown whether T9sP is functional *in vivo* and whether T9sP may have some side effects. 5) As the antitumor effect of T9sP was mild, is it possible that a combination of T9sP with chemotherapy or radiotherapy will have synergistic effects? Overall, these questions should be addressed before T9sP is developed into a novel peptide drug.

In conclusion, this work provides preliminary evidence to support the possibility that T9sP may be further developed into an innovative peptide for the treatment of glioma. In the future, additional well-designed experiments should be carried out.

Supplementary information is available in the online version of the paper.

Acknowledgments: This research was funded by the Natural Science Foundation of Jiangsu Province (BK20181156), the Top-notch Innovative Talent Project of Jiangsu Commission of Health (LGY2019020), and the Youth Talent Science and Technology Project of Changzhou Health Commission (QN202011).

References

- WELLER M, VAN DEN BENT M, TONN JC, STUPP R, PREUSSER M et al. European Association for Neuro-Oncology (EANO) guideline on the diagnosis and treatment of adult astrocytic and oligodendroglial gliomas. *Lancet Oncol* 2017; 18: e315–e329. [https://doi.org/10.1016/S1470-2045\(17\)30194-8](https://doi.org/10.1016/S1470-2045(17)30194-8)
- LOUIS DN, PERRY A, REIFENBERGER G, VON DEIMLING A, FIGARELLA-BRANGER D et al. The 2016 World Health Organization Classification of Tumors of the Central Nervous System: a summary. *Acta Neuropathol* 2016; 131: 803–820. <https://doi.org/10.1007/s00401-016-1545-1>
- LIN L, CAI J, JIANG C. Recent Advances in Targeted Therapy for Glioma. *Curr Med Chem* 2017; 24: 1365–1381. <https://doi.org/10.2174/0929867323666161223150242>
- BERNTSSON SG, MERRELL RT, AMIRIAN ES, ARMSTRONG GN, LACHANCE D et al. Glioma-related seizures in relation to histopathological subtypes: a report from the glioma international case-control study. *J Neurol* 2018; 265: 1432–1442. <https://doi.org/10.1007/s00415-018-8857-0>
- LEE A, YOUSSEF I, OSBORN VW, SAFDIEH J, BECKER DJ et al. The utilization of MGMT promoter methylation testing in United States hospitals for glioblastoma and its impact on prognosis. *J Clin Neurosci* 2018; 51: 85–90. <https://doi.org/10.1016/j.jocn.2018.02.009>
- SANAI N, BERGER MS. Glioma extent of resection and its impact on patient outcome. *Neurosurgery* 2008; 62: 753–764; discussion 264–266. <https://doi.org/10.1227/01.neu.0000318159.21731.cf>
- STUPP R, MASON WP, VAN DEN BENT MJ, WELLER M, FISHER B et al. Radiotherapy plus concomitant and adjuvant temozolomide for glioblastoma. *N Engl J Med* 2005; 352: 987–996. <https://doi.org/10.1056/NEJMoa043330>

- [8] GUO RM, ZHAO CB, LI P, ZHANG L, ZANG SH et al. Overexpression of CLEC18B Associates With the Proliferation, Migration, and Prognosis of Glioblastoma. *ASN Neuro* 2018; 10: 1759091418781949. <https://doi.org/10.1177/1759091418781949>
- [9] LIU X, WU F, JI Y, YIN L. Recent Advances in Anti-cancer Protein/Peptide Delivery. *Bioconjug Chem* 2019; 30: 305–324. <https://doi.org/10.1021/acs.bioconjchem.8b00750>
- [10] FISHER E, PAVLENKO K, VLASOV A, RAMENSKAYA G. Peptide-Based Therapeutics for Oncology. *Pharmaceut Med* 2019; 33: 9–20. <https://doi.org/10.1007/s40290-018-0261-7>
- [11] SENATUS PB, LI Y, MANDIGO C, NICHOLS G, MOISE G et al. Restoration of p53 function for selective Fas-mediated apoptosis in human and rat glioma cells in vitro and in vivo by a p53 COOH-terminal peptide. *Mol Cancer Ther* 2006; 5: 20–28. <https://doi.org/10.1158/1535-7163.MCT-05-0181>
- [12] ABDEL-SALAM MAL, CARVALHO-TAVARES J, GOMES KS, TEIXEIRA-CARVALHO A, KITTEN GT et al. The synthetic peptide LyeTxI-b derived from *Lycosa erythrognatha* spider venom is cytotoxic to U-87 MG glioblastoma cells. *Amino Acids* 2019; 51: 433–449. <https://doi.org/10.1007/s00726-018-2678-4>
- [13] LONG Q, LI L, WANG H, LI M, WANG L et al. Novel peptide dermaseptin-PS1 exhibits anticancer activity via induction of intrinsic apoptosis signalling. *J Cell Mol Med* 2019; 23: 1300–1312. <https://doi.org/10.1111/jcmm.14032>
- [14] SWENSON S, MINEA RO, TUAN CD, THEIN TZ, CHEN TC et al. A Novel Venom-Derived Peptide for Brachytherapy of Glioblastoma: Preclinical Studies in Mice. *Molecules* 2018; 23: 2918. <https://doi.org/10.3390/molecules23112918>
- [15] LIU K, ZHANG C, LI B, XIE W, ZHANG J et al. Mutual Stabilization between TRIM9 Short Isoform and MKK6 Potentiates p38 Signaling to Synergistically Suppress Glioblastoma Progression. *Cell Rep* 2018; 23: 838–851. <https://doi.org/10.1016/j.celrep.2018.03.096>
- [16] JARAÍZ-RODRÍGUEZ M, TALAVERÓN R, GARCÍA-VICENTE L, PELAZ SG, DOMÍNGUEZ-PRIETO M et al. Connexin43 peptide, TAT-Cx43266-283, selectively targets glioma cells, impairs malignant growth, and enhances survival in mouse models in vivo. *Neuro Oncol* 2020; noaa087. <https://doi.org/10.1093/neuonc/noaa087>
- [17] ZHI F, ZHOU G, SHAO N, XIA X, SHI Y et al. miR-106a-5p Inhibits the Proliferation and Migration of Astrocytoma Cells and Promotes Apoptosis by Targeting FASTK. *PLoS One* 2013; 8: e72390. <https://doi.org/10.1371/journal.pone.0072390>
- [18] LEVIN VA, TONGE PJ, GALLO JM, BIRTWISTLE MR, DAR AC et al. CNS Anticancer Drug Discovery and Development Conference White Paper. *Neuro Oncol* 2015; 17: vi1-26. <https://doi.org/10.1093/neuonc/nov169>
- [19] NEUHAUS CS, GABERNET G, STEUER C, ROOT K, HISS JA et al. Simulated Molecular Evolution for Anticancer Peptide Design. *Angew Chem Int Ed Engl* 2019; 58: 1674–1678. <https://doi.org/10.1002/anie.201811215>
- [20] BAJRACHARYA R, SONG JG, BACK SY, HAN HK. Recent Advancements in Non-Invasive Formulations for Protein Drug Delivery. *Comput Struct Biotechnol J* 2019; 17: 1290–1308. <https://doi.org/10.1016/j.csbj.2019.09.004>
- [21] LAGASSÉ HAD, ALEXAKI A, SIMHADRI VL, KATAGIRI NH, JANKOWSKI W et al. Recent advances in (therapeutic protein) drug development. *F1000Res* 2017; 6: 113. <https://doi.org/10.12688/f1000research.9970.1>
- [22] FUJITA M, SASADA M, IYODA T, FUKAI F. Involvement of Integrin-Activating Peptides Derived from Tenascin-C in Cancer Aggression and New Anticancer Strategy Using the Fibronectin-Derived Integrin-Inactivating Peptide. *Molecules* 2020; 25: 3239. <https://doi.org/10.3390/molecules25143239>
- [23] SU BC, WU TH, HSU CH, CHEN JY. Distribution of positively charged amino acid residues in antimicrobial peptide epinecidin-1 is crucial for in vitro glioblastoma cytotoxicity and its underlying mechanisms. *Chem Biol Interact* 2020; 315: 108904. <https://doi.org/10.1016/j.cbi.2019.108904>
- [24] SU BC, PAN CY, CHEN JY. Antimicrobial Peptide TP4 Induces ROS-Mediated Necrosis by Triggering Mitochondrial Dysfunction in Wild-Type and Mutant p53 Glioblastoma Cells. *Cancers (Basel)* 2019; 11: 171. <https://doi.org/10.3390/cancers11020171>
- [25] VARANKO A, SAHA S, CHILKOTI A. Recent trends in protein and peptide-based biomaterials for advanced drug delivery. *Adv Drug Deliv Rev* 2020; 156: 133–187. <https://doi.org/10.1016/j.addr.2020.08.008>
- [26] PUCCI C, DE PASQUALE D, MARINO A, MARTINELLI C, LAUCIELLO S et al. Hybrid Magnetic Nanovectors Promote Selective Glioblastoma Cell Death through a Combined Effect of Lysosomal Membrane Permeabilization and Chemotherapy. *ACS Appl Mater Interfaces* 2020; 12: 29037–29055. <https://doi.org/10.1021/acsami.0c05556>
- [27] LIN YL, HUANG XF, CHANG KF, LIAO KW, TSAI NM. Encapsulated n-Butylideneephthalide Efficiently Crosses the Blood-Brain Barrier and Suppresses Growth of Glioblastoma. *Int J Nanomedicine* 2020; 15: 749–760. <https://doi.org/10.2147/IJN.S235815>
- [28] LINGASAMY P, TOBI A, KURM K, KOPANCHUK S, SUDAKOV A et al. Tumor-penetrating peptide for systemic targeting of Tenascin-C. *Sci Rep* 2020; 10: 5809. <https://doi.org/10.1038/s41598-020-62760-y>
- [29] WANG X, MENG N, WANG S, ZHANG Y, LU L et al. Non-immunogenic, low-toxicity and effective glioma targeting MTI-31 liposomes. *J Control Release* 2019; 316: 381–392. <https://doi.org/10.1016/j.jconrel.2019.11.005>
- [30] AGARWAL S, MOHAMED MS, MIZUKI T, MAEKAWA T, SAKTHI KUMAR D. Chlorotoxin modified morusin-PLGA nanoparticles for targeted glioblastoma therapy. *J Mater Chem B* 2019; 7: 5896–5919. <https://doi.org/10.1039/c9tb01131e>
- [31] CHAI Z, RAN D, LU L, ZHAN C, RUAN H et al. Ligand-Modified Cell Membrane Enables the Targeted Delivery of Drug Nanocrystals to Glioma. *ACS Nano* 2019; 13: 5591–5601. <https://doi.org/10.1021/acs.nano.9b00661>
- [32] YUAN BO, ZHAO Y, DONG S, SUN Y, HAO F et al. Cell-penetrating Peptide-coated Liposomes for Drug Delivery Across the Blood-Brain Barrier. *Anticancer Res* 2019; 39: 237–243. <https://doi.org/10.21873/anticancer.13103>

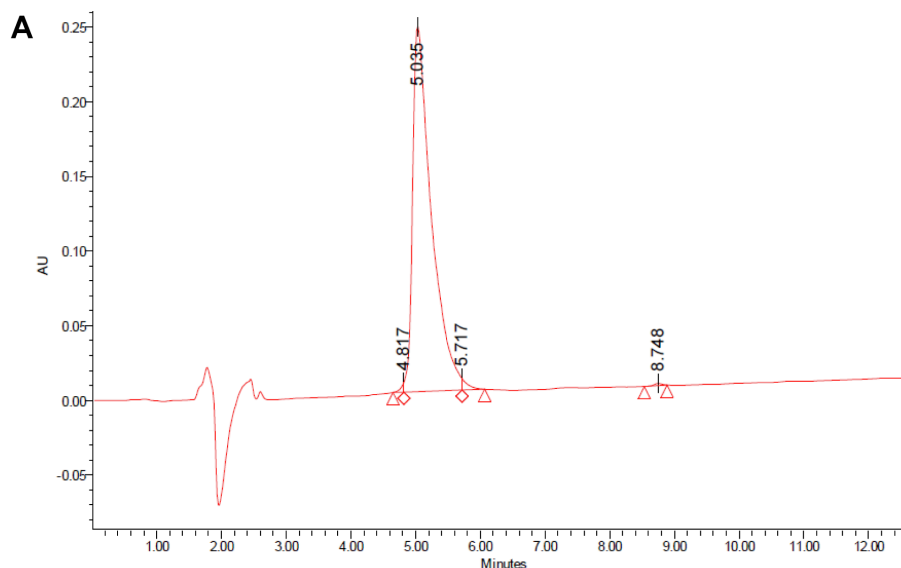
- [33] LEE AC, HARRIS JL, KHANNA KK, HONG JH. A Comprehensive Review on Current Advances in Peptide Drug Development and Design. *Int J Mol Sci* 2019; 20: 2383. <https://doi.org/10.3390/ijms20102383>
- [34] EVERS A, PFEIFFER-MAREK S, BOSSART M, HEUBEL C, STOCK U et al. Peptide Optimization at the Drug Discovery-Development Interface: Tailoring of Physicochemical Properties Toward Specific Formulation Requirements. *J Pharm Sci* 2019; 108: 1404–1414. <https://doi.org/10.1016/j.xphs.2018.11.043>
- [35] TESAURO D, ACCARDO A, DIAFERIA C, MILANO V, GUILLON J et al. Peptide-Based Drug-Delivery Systems in Biotechnological Applications: Recent Advances and Perspectives. *Molecules* 2019; 24: 351. <https://doi.org/10.3390/molecules24020351>

https://doi.org/10.4149/neo_2021_201109N1196

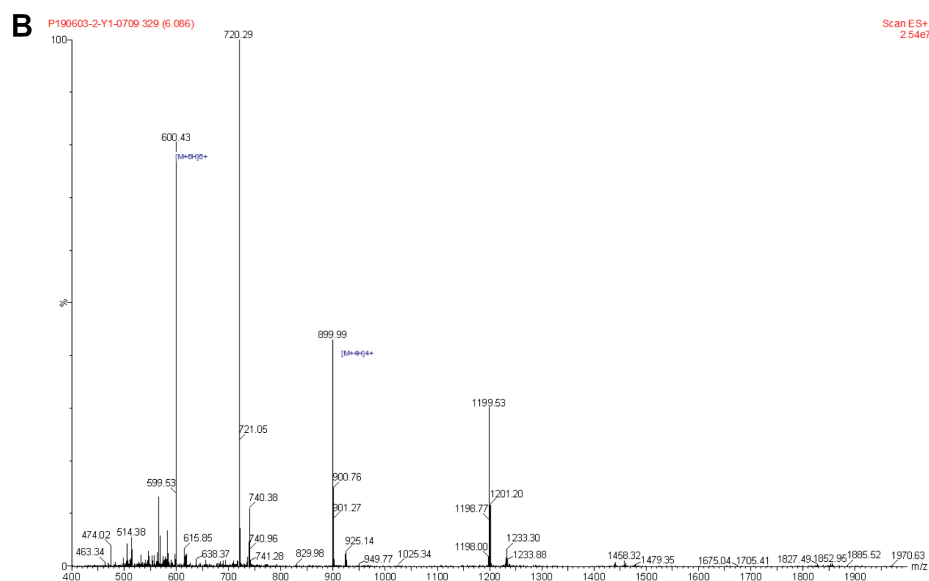
A novel antitumor peptide inhibits proliferation and migration and promotes apoptosis in glioma cells by regulating the MKK6/p38 signaling pathway

Rong WANG^{1,2,†}, Bo-Wen LI^{2,†}, Nai-Yuan SHAO¹, Dan-Ni DENG², Feng ZHI^{1,2,*}

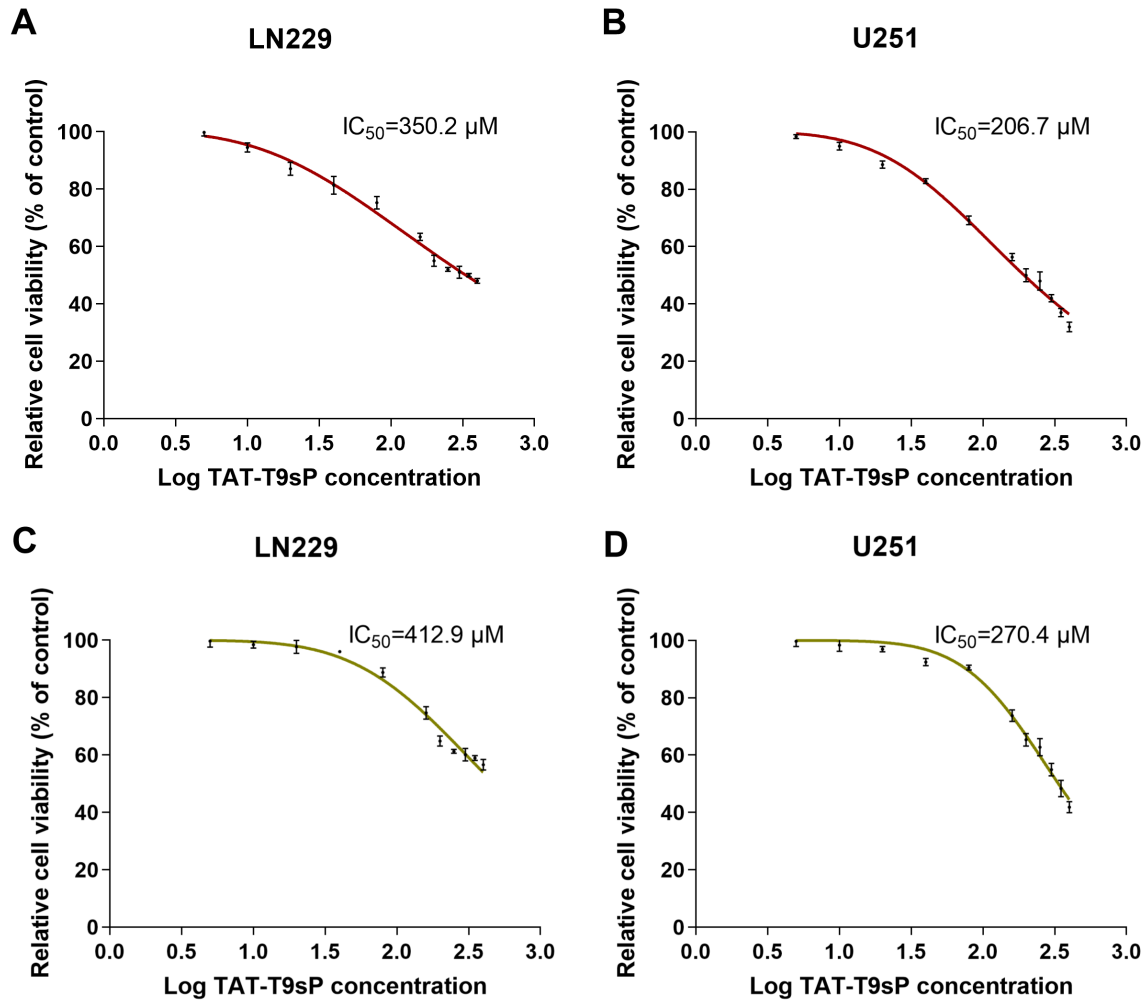
Supplementary Information



	Processed Channel	Retention Time (min)	Area	% Area	Height
1	2487Channel 1	4.817	19201	0.38	6468
2	2487Channel 1	5.035	4910565	98.44	244699
3	2487Channel 1	5.717	47132	0.94	7678
4	2487Channel 1	8.748	11586	0.23	1412



Supplementary Figure S1. UHPLC chromatogram (A) and mass spectrum (B) of TAT-T9sP.



Supplementary Figure S2. Cell viability assay. A) The relative cell viability of LN229 cells after treated by different concentrations of TAT-T9sP. B) The relative cell viability of U251 cells after treated by different concentrations of TAT-T9sP. C) The relative cell viability of LN229 cells after treated by different concentrations of TAT-T9sP combined with SB203580. D) The relative cell viability of U251 cells after treated by different concentrations of TAT-T9sP combined with SB203580. Each experiment was repeated 3 times.